Processed foods

Paradoxically India ranks in the bottom ten countries of the world in the international food market in spite of the fact that every fourth farmer globally is an Indian. Less than 1.0% of the total agricultural production is converted into processed products. On an average an Indian spends 52.4% of his earnings on food. The net disposable income is increasing. There is a great influx of people to the urban areas which contributes to the growth of consumer industry. Use of processed foods in Indian households has been a recent trend.

The factors that influence the marketing of processed foods in India can be attributed to the negative disposition of the consumer who is used to traditional foods. Quality problems of products and limited product range have also affected the growth of food industries. This trend can be reversed only by creating greater consumer awareness on processed foods, right product positioning and packaging with affordable price to the consumers. The export performance of the processed food products industry is likely to grow in coming years.

Conclusion

'Food for the future' and attaining self-sufficiency by the turn of the century is primarily dependent on the availability of adequate finances. There are several proposals to improve the food front prepared by experts with the government which need to be implemented. Food strategy for 2000 AD needs specific shifts in farm strategies which include modification of energy, intensive hybrid variety technologies, gradual shift from fine to coarse grains, changes in cropping pattern to match agro-soil-climate and new agricultural technology. The basic truth to be realized in the context of rural Indian economy is that the farmers will not grow crops if prices of produce remain low and subsidies benefit only the urban population and this needs to be phased out. Farmers will improve their land only if they own it and this must not be merely ideological but must become real. The present decade is crucial both in controlling population growth and reaching food sufficiency by all-round efforts for a strong India.

REVIEW ARTICLE

Synthesis and characterization of fullerenes C_{60} and C_{70} and superconductivity in K and Rb-doped C_{60}

Y. Hariharan, A. Bharathi, C. S. Sundar, V. S. Sastry, M. Yousuf, T. S. Radhakrishnan, G. V. N. Rao, T. GeethaKumary, N. Subramanian, P. Ch. Sahu, V. S. Raghunathan* and M. C. Valsakumar

Materials Science Division, *Metallurgy Division, Indira Gandhi Centre for Atomic Research, Kalpakkam 603 102, India

The synthesis of fullerenes C_{60} and C_{70}, its characterization and alkali doping of C_{60} are described in detail. K- and Rb-doped C_{60} are observed to be superconducting with T_c of 18 K and 27 K respectively. Bi and Pb have been co-doped along with K and the results of structure and superconductivity studies in these systems are presented and discussed. Further, preliminary results of on-going experiments on the structure of C_{70} and its variation with temperature and pressure are also presented.

KROTO *et al.*[1] in 1985 discovered the existence of stable carbon clusters of 60 atoms in the mass spectrum of laser-ablated graphite, for which they proposed a soccer ball structure and termed it as buckminsterfullerene after the designer of geodesic domes. The recent synthesis of macroscopic quantities of fullerenes by Kratschmer *et al.*[2] by striking an arc between graphite electrodes in a helium atmosphere has generated a flurry of interest in the close caged carbon molecules C_{60}, C_{70} and in the study of their solid state properties. The study of fullerenes received further impetus with the initial discovery of metallicity[3] in alkali metal doped C_{60} and the subsequent announcement of superconductivity[4,5] in C_{60} doped with K ($T_c = 18$ K), Rb[6] ($T_c = 28$ K), Cs[7] and their alloys[8,9]. Following these

results, intensive experimental and theoretical effort is being made to understand the mechanism of superconductivity in the alkali metal doped C_{60}. The structure[10,11], electronic[12,13] and vibrational[14,15] properties of undoped and doped C_{60} have been investigated. The properties in the superconducting state such as the critical fields[16], coherence length[16], penetration depth[16,17] and the superconducting energy gap[18,19] have been obtained. In addition to studies on alkali metal-doped C_{60}, experiments with other dopants are also being carried out with a view to increasing T_c and also to obtain an understanding of the mechanism of superconductivity. For example, superconductivity at 45 K has been observed[20] when Tl is co-doped along with Rb. Recently, it has been shown[21] that Ca can be doped into C_{60} and the resultant sample is superconducting with $T_c = 8.4$ K.

In this article, we present the details of the synthesis and characterization of C_{60} and C_{70}. Doping of C_{60} with alkali metals K and Rb, and the results of our studies on structure and superconductivity in these systems are then described. While the material presented in these sections is not new, it helps to provide a review and a detailed comparison with the procedures employed by other research groups. Following the earlier studies[20] on co-doping of Tl along with K and Rb into C_{60}, we have doped Pb and Bi along with K into C_{60}. The results of structure and superconductivity studies in these systems are presented and discussed. In addition, preliminary results of on-going studies on the structure of C_{70} and its variation with pressure and temperature are also indicated.

Synthesis of fullerenes

The synthesis of fullerenes involves first the production of carbon soot, which is mainly done either by resistive heating of graphite electrodes or 'contact arc' between graphite electrodes[2,22–24]. Other methods such as burning of benzene in flame have also been reported[25]. The carbon clusters contained in the soot are then extracted in toluene and chromatographically separated to obtain C_{60} and C_{70}. The flow chart for the synthesis of fullerenes and their doping with alkali metals is shown in Figure 1.

SYNTHESIS AND DOPING OF FULLERENES

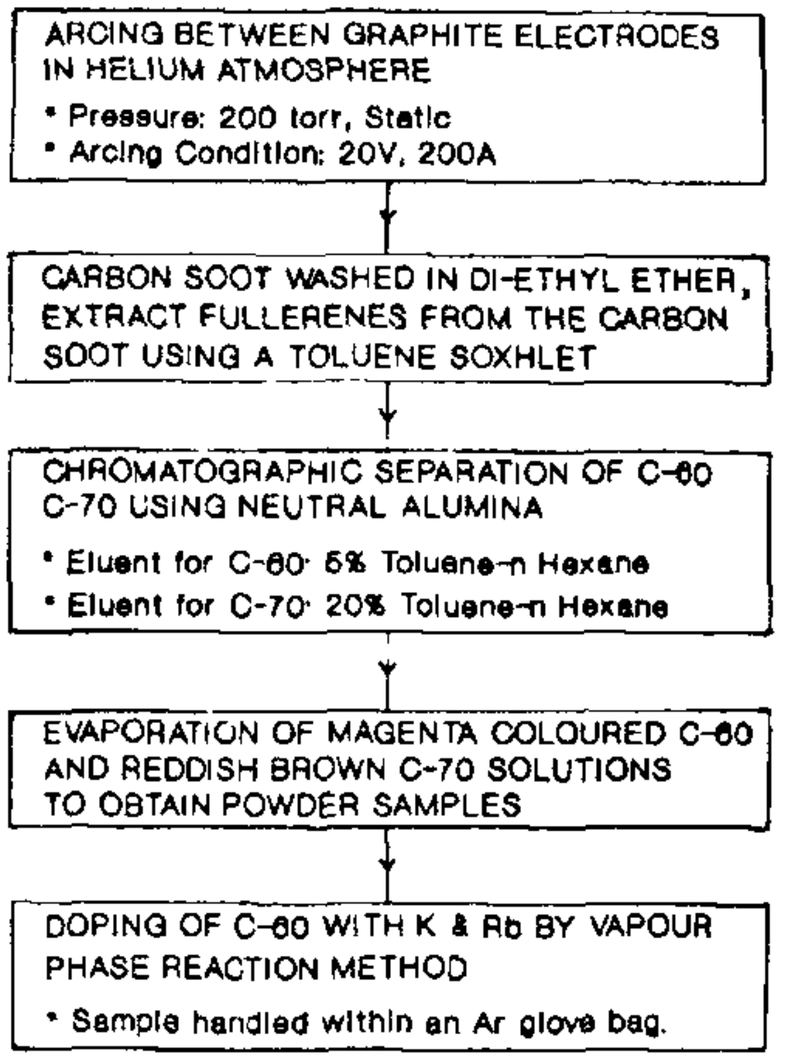

Figure 1. Flow chart for the synthesis and doping of fullerenes.

Arcing of graphite electrodes

The schematic of the apparatus used for the production of carbon soot is shown in Figure 2. It consists of a pair of water-cooled graphite electrodes between which an arc is struck in a helium atmosphere. The electrodes are enclosed in a water-cooled chamber which can be evacuated by a rotary pump with liquid nitrogen trap and subsequently refilled with helium to the desired pressure. An important design feature of this set up is that one of the electrodes can be moved inside the vacuum/helium atmosphere through a wilson seal by a lead screw arrangement. The electrodes are connected to a low voltage (40 volts max.), high current (400 Å max.) AC power supply with the live end connected to the stationary electrode.

To generate the carbon soot, the system is evacuated to 10^{-2} torr, purged twice with helium gas and refilled with helium to 200 torr. After the initial resistive heating, when the electrodes are in contact with each other, the movable electrode is retracted such that a bright arc with a gap of approximately 3 mm is maintained. The movable electrode that gets consumed is moved progressively to maintain the bright arc. At the end of each operation, lasting about 4 h, approximately 20 cm of the movable electrode is consumed and 10 g of soot is collected from the inner walls of the vacuum chamber.

During the operation of this apparatus, the influence of various parameters such as the helium pressure, the nature of graphite rods, the operating current and voltage, etc., on the quality and yield of soot have been tried. Helium pressure has been varied between 100 and 300 torr with the best results obtained for 200 torr. Both static and dynamic (controlled leak rate) helium conditions have been tried and best performance was seen under the former. The experiments on the variation of operating voltage indicated that for 10-mm graphite rods best performance was seen under the operating condition of 20 V, 200 Å. The performance of

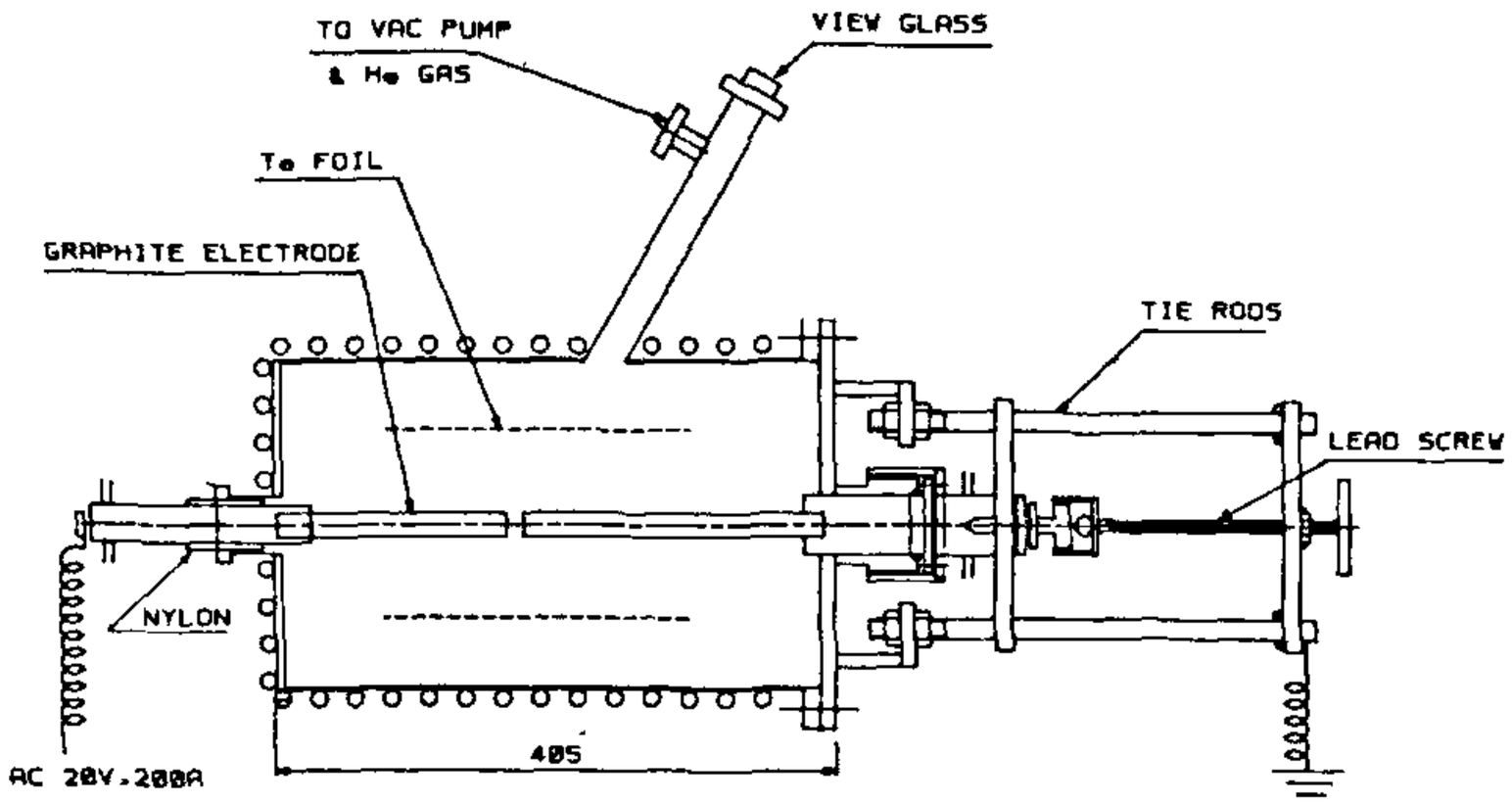

Figure 2. Schematic of the graphite arcing apparatus.

this system improved significantly after the incorporation of a perforated tantalum sheet above the electrodes (see Figure 2). Whether it is due to the avoidance of photo-disintegration[26] or due to the longer retention of the carbon vapours in the region of the arc, thus enabling the formation of fullerene molecules[27], is not clear at the moment.

Separation of C_{60} and C_{70}

The soot collected from the arcing apparatus is packed in a filter paper and then introduced in the Soxhlet apparatus containing toluene. In ~24 h of operation, a reddish brown solution containing fullerenes in toluene was obtained. This was concentrated by evaporation in a distillation apparatus at 120°C. Chromatographic separation of C_{60} and C_{70} was achieved using a column, 1 meter long and 3.5 cm diameter, in which 500 g of neutral grade alumina was loaded. The alumina was heat-treated at 200°C for 24 h to get rid of all the moisture before packing into the chromatographic column. The column was conditioned with *n*-hexane and then the Soxhlet extract (5% solution in *n*-hexane) was poured into the column. A clear separation of purple and brown bands corresponding to C_{60} and C_{70} was seen. C_{60} was eluted using a 5% toluene–*n*-hexane mixture resulting in the collection of a clear magenta-coloured solution. This was followed by the elution of a clear solution, after which the reddish brown C_{70} solution was eluted out using a 20% toluene–*n*-hexane mixture. The eluents obtained at various stages of chromatography were characterized for the presence of C_{60} and C_{70} by ultraviolet-visible absorption spectroscopy (see next section). The magenta solution was evaporated to get rid of *n*-hexane and toluene. The residue is washed in diethyl ether and centrifuged to obtain black crystallites of C_{60}. A similar operation with the reddish brown solution yielded the C_{70} powder. The average yield of C_{60} and C_{70} powder together was observed to be ~5%, with C_{60} and C_{70} in the ratio of 80:20. This is the typical yield obtained in many experiments, though yields as high[22] as 44% of soluble fullerenes and even 100% yield[24] of C_{60} during arcing have been reported. In addition to the use of toluene for extraction of fullerenes, as described here, benzene has also been extensively used as the solvent. Parker *et al*[22] have compared the use of various solvents such as benzene, pyridine, tetramethyl benzene on the yield of fullerenes. Further, in addition to the use of alumina column, silica gel[3,29] has also been used in the chromatographic separation of C_{60} and C_{70}.

Characterization

Several experimental techniques have been used to characterize and study the fullerenes. These include mass spectrometry[2,28], optical absorption in the infra-red, visible and ultraviolet[2,29], X-ray diffraction[2,10], Raman spectroscopy[3,30] and NMR[31]. In our experiments, the chromatographically separated C_{60} and C_{70} have been characterized by ultraviolet-visible absorption spectroscopy, X-ray diffraction and scanning electron microscopy.

The optical absorption spectrum in the UV-visible range was carried out on the separated C_{60} and C_{70} dissolved in *n*-hexane using a Shimadzu, model UV-240, spectrometer. The absorption spectrum recorded at room temperature in the range of 300 nm-700 nm is shown in Figure 3. The spectra of C_{60} show dominant absorption band at 328 nm and a double-hump structure centred at 404 and 408 nm respectively. In the case of C_{70}, broad humps are seen at 550 nm, 470 nm

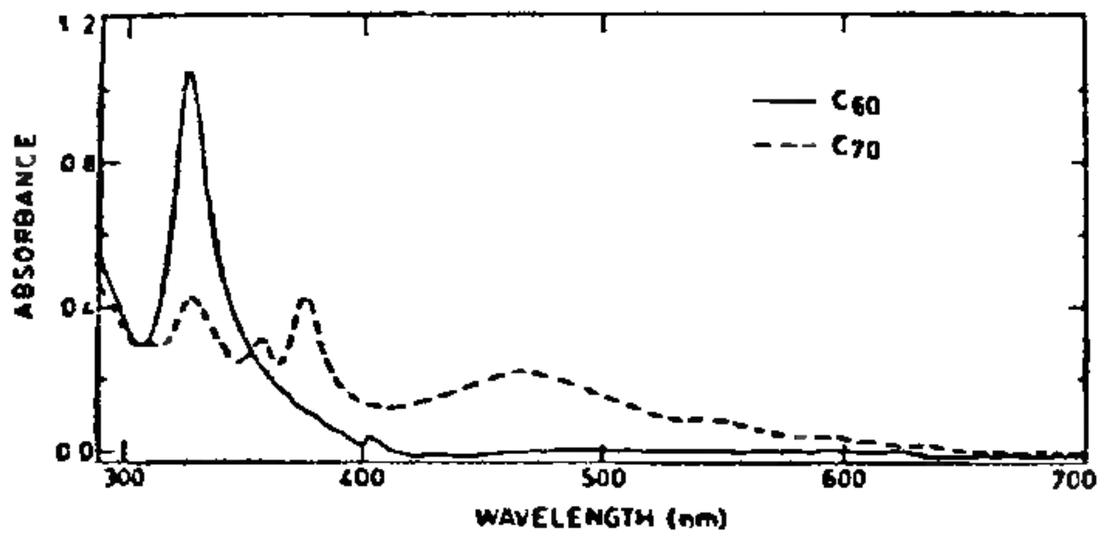

Figure 3. Absorption spectra of C_{60} and C_{70} in *n*-hexane in the range 300–700 nm.

and in the near-UV region at 378 nm, 359 nm and 331 nm. The dominant spectral features in C_{60} and C_{70} are in agreement with those reported by Ajie *et al*[29]. As a test of the efficacy of chromatographic separation, in particular the possible contamination of C_{60} in C_{70}, the absorption spectra were recorded with higher sensitivity in the range of 380–430 nm (see Figure 4). The characteristic double-hump structure seen in the absorption spectrum of C_{60} cannot be discerned in the spectrum of C_{70}. On the basis of this, the content of C_{60} in the chromatographically separated C_{70} is estimated to be less than 2%.

The icosahedral C_{60} molecules have been shown[10] to crystallize in the fcc structure with complete orientational disorder at room temperature, the orientational order developing at temperature less than 249 K. The room temperature X-ray diffraction pattern of C_{60} powder measured using CuK_α radiation is shown in Figure 5. The diffraction pattern could be indexed to fcc structure with a lattice constant of 14.2±0.1 Å. Further,

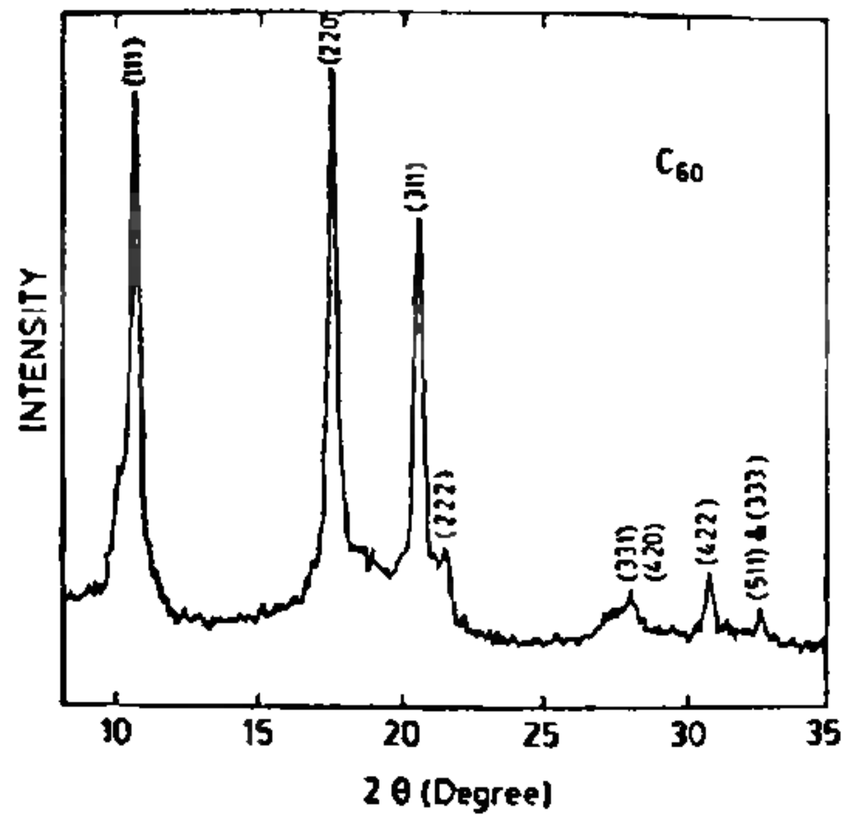

Figure 5. X-ray diffraction pattern of C_{60}. The diffraction lines have been indexed to fcc structure.

as noted in ref. 32, it is seen that the diffraction peak corresponding to (200) index is not observed. This arises[32] due to the accidental vanishing of molecular form factor when hollow spherical C_{60} clusters of radius r (3.55 Å) are packed in a fcc lattice with a lattice constant of 4* r (14.2 Å).

Figure 6 shows the scanning electron micrograph of C_{60} crystallites obtained from the slow evaporation of C_{60} powder dissolved in toluene. These micrographs were taken using Philips model PSEM -501, on C_{60} crystallites coated with Au to induce conductivity. The micrograph clearly shows the cubic morphology of the crystallites and the close packed (111) planes. The average crystallite size is seen to be ~40 μm.

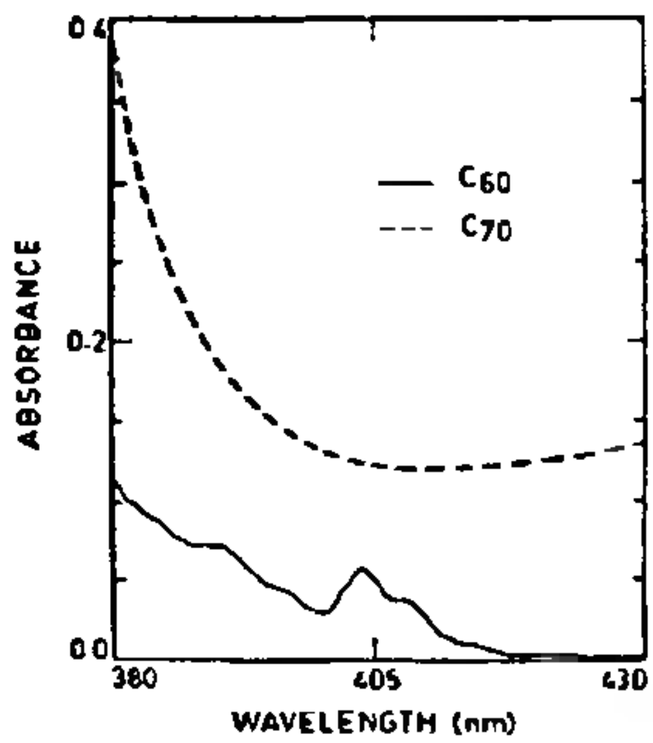

Figure 4. Absorption spectra of C_{60} and C_{70}, measured with an enhanced sensitivity in the range 380 to 430 nm. Note that the characteristic double hump structure of C_{60} around 405 nm is not seen in the spectrum of C_{70}, indicating the efficacy of the chromatographic separation.

Figure 6. Scanning electron micrograph of C_{60}. The cubic morphology of the crystallites and the associated close packed (111) planes can be clearly seen.

Alkali metal doping of C_{60}

In the first report[4] of superconductivity ($T_c = 18$ K) in K-doped C_{60} films, the doping was carried out by the vapour phase reaction method. Holczer *et al*[5] have described in detail the protocol for the doping of K (and Rb) in bulk C_{60}. From the studies on the diamagnetic shielding as a function of initial K composition, they have identified the composition of the superconducting phase to be K_3C_{60}. Stephens *et al.*[11] have determined the structure of K_3C_{60} to be fcc with the K atoms located at the tetrahedral and octahedral holes of the fcc C_{60} lattice. In addition to the fcc phase K_3C_{60} which is superconducting, bct phase[33] K_4C_{60} and bcc phase[34] K_6C_{60}, both of which are nonsuperconducting are also formed in K-doped C_{60}. Following the results in K-doped C_{60}, superconductivity has also been observed in Rb-doped[5,6] C_{60} ($T_c = 28$ K), Cs-doped[7] C_{60} ($T_c = 30$ K), and on doping with alloys[8,9] of K, Rb and Cs. The T_c is observed[35] to increase with the lattice parameter of the fcc superconducting phase.

Since the initial report of the preparation of K-doped C_{60} by the vapour phase reaction method, other synthesis procedures have been tried out with a view to obtaining better control over the stoichiometry, and to increase the superconducting volume fraction. The difficulties in the handling of small quantities of air-sensitive alkali metals inside a dry box have been overcome to some extent by treating C_{60} with alkali/heavy metal amalgams[7]. Another method[36] to obtain better control over the stoichiometry involves first the preparation of saturation product (K_6C_{60}), which is subsequently reacted with known amount of C_{60} to obtain K_3C_{60}. A solution route for the synthesis of K-doped C_{60} has been described by Wang *et al.*[37] in which C_{60} dissolved in toluene is reacted with K chips in an air-free environment.

In the present experiments, stoichiometric quantities of C_{60} and K (corresponding to the composition K_3C_{60}) were loaded into a 6 mm dia, 20 cm long pyrex tube fitted with a stop cock. The mixture (~20 mg) was heat-treated in vacuum (10^{-5} torr) at 250° C for 24 h. The mixture was reground and heat-treated again in vacuum at 250° C for 24 h. The reaction product was loaded into the teflon capsule for AC susceptibility measurements. Finely ground powder was loaded into a Lindemann glass capillary and sealed for X-ray measurements. All operations involving handling of the sample were carried out inside an argon-filled glove bag, wherein the humidity was controlled.

The X-ray diffraction pattern of K-doped C_{60} is shown in Figure 7. The broad background is due to the glass capillary. The diffraction lines could be indexed to a fcc structure. The diffraction lines corresponding to K are also indexed and it is seen that very small amount

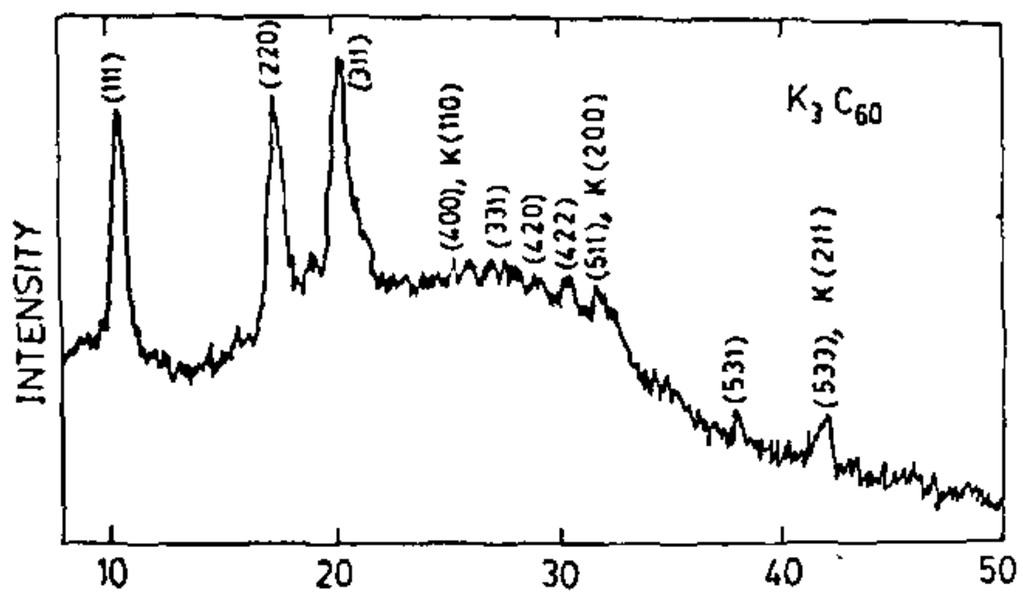

Figure 7. X-ray diffraction pattern of K doped C_{60}. The diffraction lines have been indexed to fcc structure. The diffraction lines corresponding to K are also indicated.

of unreacted K, if any, is present. The lattice constant is estimated to be 14.3 ± 0.1 Å and is seen to be marginally larger than in undoped C_{60}. Comparing with the diffraction pattern of C_{60} (see Figure 5), it is seen that the dominant change due to K doping is in the relative intensities of the (220) and (311) diffraction lines. As indicated by Stephens *et al*[11], this arises due to doping of K at (1/4, 1/4, 1/4) and (1/2, 0, 0) positions in the unit cell.

AC susceptibility measurements were carried out at 941 Hz using a mutual inductance coil and lock-in amplifier. The variation of normalized susceptibility as a function of temperature, as measured using a calibrated carbon resistor, shows a sharp superconducting transition (cf. Figure 8) with a onset at 18 K and a transition width (25 to 75%) of 3 K. The superconducting volume fraction with respect to Nb standard is estimated to be 10%. This is somewhat smaller than the volume fraction reported by Fleming *et al.*[35] (28.6%), Holczer *et al.*[5] (30%) and McCauley *et al.*[36] (38%).

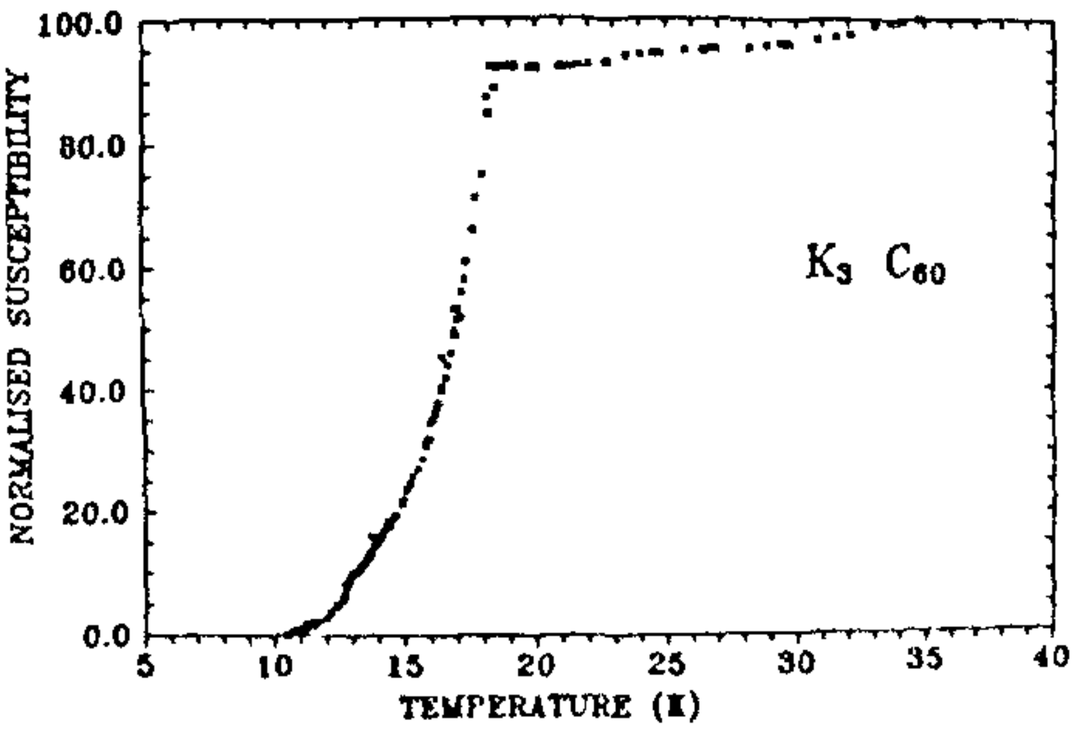

Figure 8. Normalized susceptibility versus temperature in K doped C_{60}, indicating the superconducting transition at 18 K.

Further work on various heat-treatment schedules to improve the superconducting volume fraction is envisaged.

Doping of C_{60} with Rb was carried out along similar lines to that of K, except that the heat treatment in this case was carried out at 440° C. Figure 9 shows the X-ray diffraction pattern of the Rb-doped C_{60}. The lines could be indexed to fcc structure with a lattice constant of 14.4 ± 0.1 Å. Comparing with the diffraction patterns of C_{60} (Figure 5), and K_3C_{60} (Figure 7), it is seen that the (200) line is present. This arises because of the expansion of the lattice so that the fortuitous condition $a = 4*r$ is no longer satisfied[32]. The results of AC susceptibility measurements on the Rb-doped sample are shown in Figure 10. A sharp superconducting transition with a T_c (onset) at 27 K is clearly seen. The superconducting volume fraction is estimated to be 7%.

Both the K- and Rb-doped samples are known to be air-sensitive and superconductivity degrades with time. For example, Holczer *et al.*[5] have reported that the Meissner fraction degrades to 50% in about 3 h and the signal vanishes in about three days. This degradation has been attributed[36] to the leaching out of K by oxygen resulting in the formation of K-oxide. This may also be related to the phase changes in the original multi-phasic compound as seen from NMR[39] experiments. We have observed that on storing the samples in vacuum at room temperature, the superconducting volume fraction degrades to about 70% of its original value over a period of 15 days (see Figure 11). However, no significant change in T_c and ΔT_c is seen. Further work on correlating the degradation of the superconducting volume fraction with the changes in structure and composition is in progress.

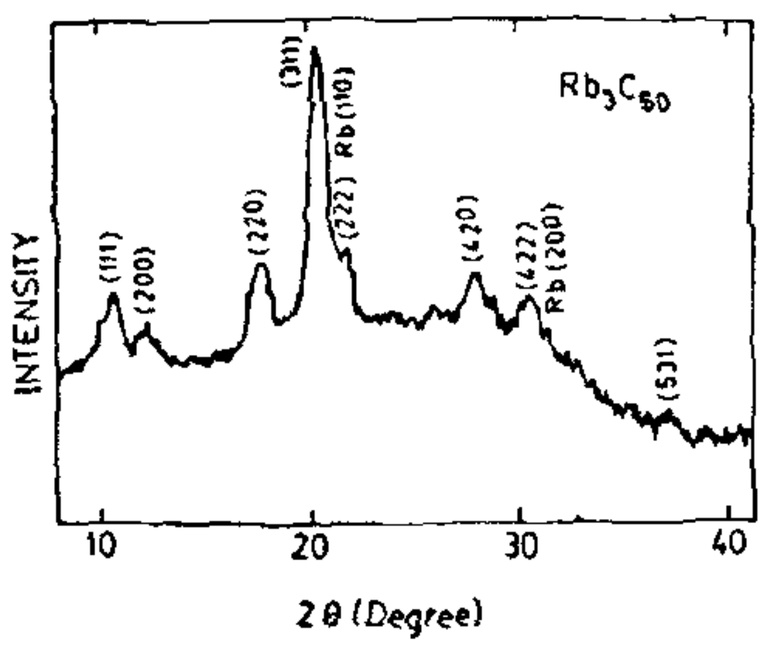

Figure 9. X-ray diffraction pattern of Rb doped C_{60}. The diffraction lines corresponding to Rb are also indicated.

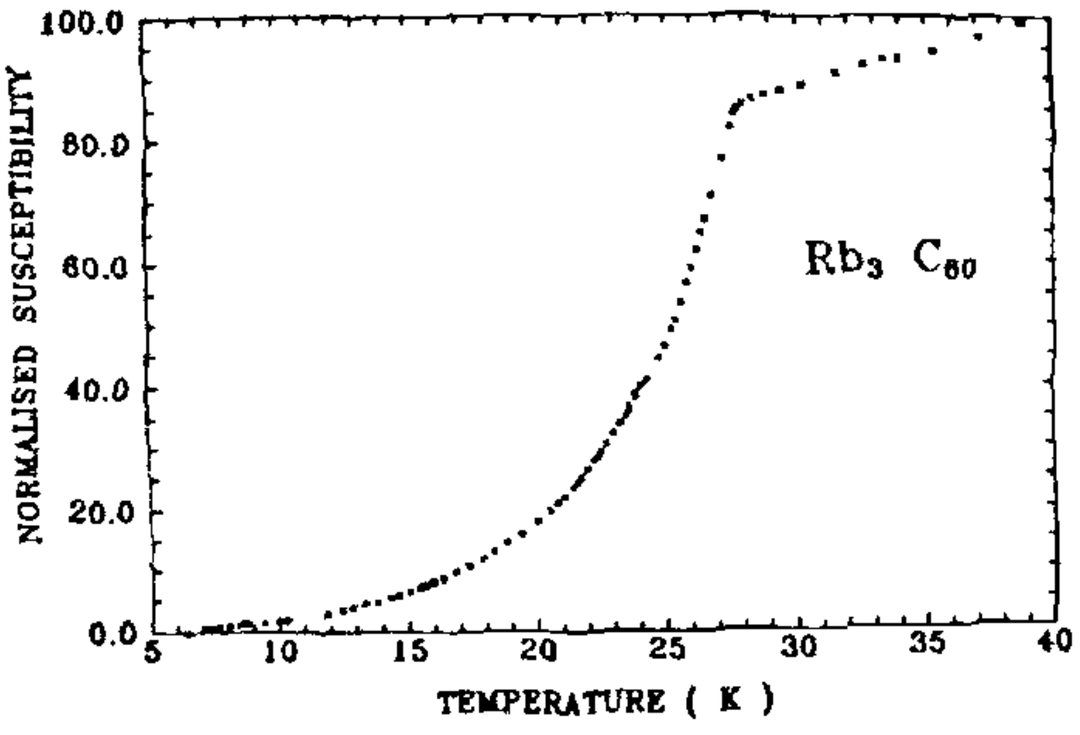

Figure 10. Normalized susceptibility versus temperature in Rb doped C_{60}, indicating superconducting transition at 27 K.

Studies on co-doping Pb and Bi along with K

In addition to doping C_{60} with alkali metals, attempts have also been made to dope with other elements and to co-dope with alkalis with a view to studying the systematics in the properties of doped C_{60} and also to increase T_c. From the studies on various alkali-doped C_{60}, it has been established[35] that T_c scales linearly with the lattice parameter of the fcc phase and this has been attributed to the increase in the density of states at the Fermi level. One of the remarkable results[20] of the co-doping studies is that on doping Tl with K, T_c is observed to increase to 25 K compared to 18 K in K_3C_{60}, and on co-doping Tl along with Rb, T_c increases dramatically to 45 K as compared to 28 K in Rb_3C_{60}. The exact reason for this observed increase in T_c is not clear at present. Following the success of Tl doping, we have attempted to co-dope Pb and Bi along with K into C_{60}. The choice of these dopants is based on similarity to Tl in important parameters such as the ionic radius, ionization potential, vapour pressure, etc., all of which possibly control the incorporation of dopant into the C_{60} lattice. For example, in Tl, Pb and Bi, the ionic radius are 1.48 Å, 1.47 Å, 1.46 Å respectively, the ionization potentials are 6.11 eV, 7.41 eV, 7.29 eV respectively and the vapour pressure at 450° C are 2×10^{-5} torr, 1×10^{-6} torr, and 3×10^{-6} torr respectively.

Samples having nominal composition of PbK_2C_{60}

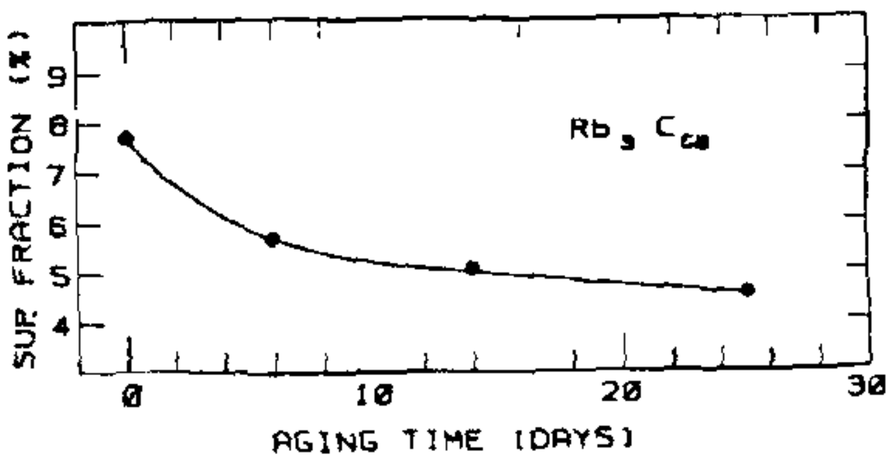

Figure 11. Variation of the superconducting volume fraction as function of ageing time for Rb_3C_{60} sample stored in vacuum at room temperature.

and BiK_2C_{60} were prepared by the vapour phase reaction starting with stoichiometric constituents. The samples were heat-treated inside a pyrex tube in vacuum at 400° C for 24 h, followed by additional heat-treatment at 450° C for 24 h. The resulting samples were characterized by X-ray diffraction and AC susceptibility measurements.

The results of AC susceptibility measurements in PbK_2C_{60} and BiK_2C_{60} are shown in Figures 12 and 13 respectively. It is seen that both these samples show sharp superconducting transition with onset at 18 K as in the case of K_3C_{60} (cf. Figure 8). Further, in the case of PbK_2C_{60} sample, the transition corresponding to unreacted Pb is also seen.

X-ray diffraction patterns in PbK_2C_{60} and BiK_2C_{60} are shown in Figure 14. Comparing with the diffraction pattern of C_{60}, also shown in the figure, it can be discerned that the diffraction lines in the doped samples are shifted towards smaller angles, indicating an

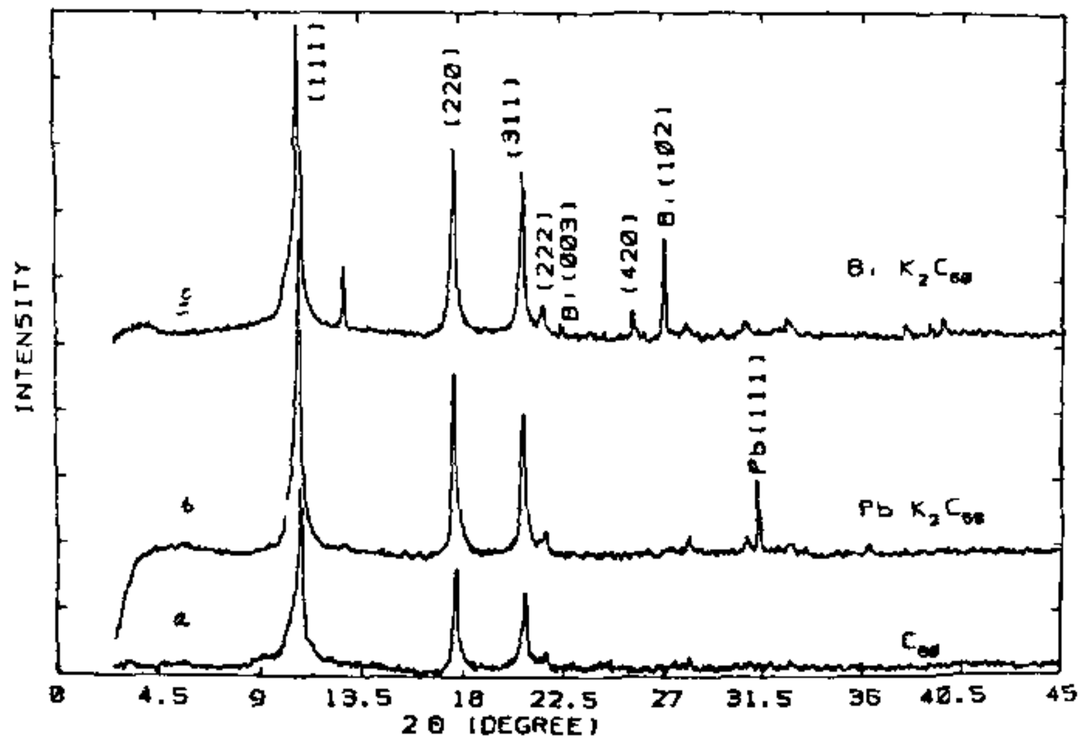

Figure 14. X-ray diffraction pattern in (*a*) C_{60}, (*b*) PbK_2C_{60}, and (*c*) BiK_2C_{60}.

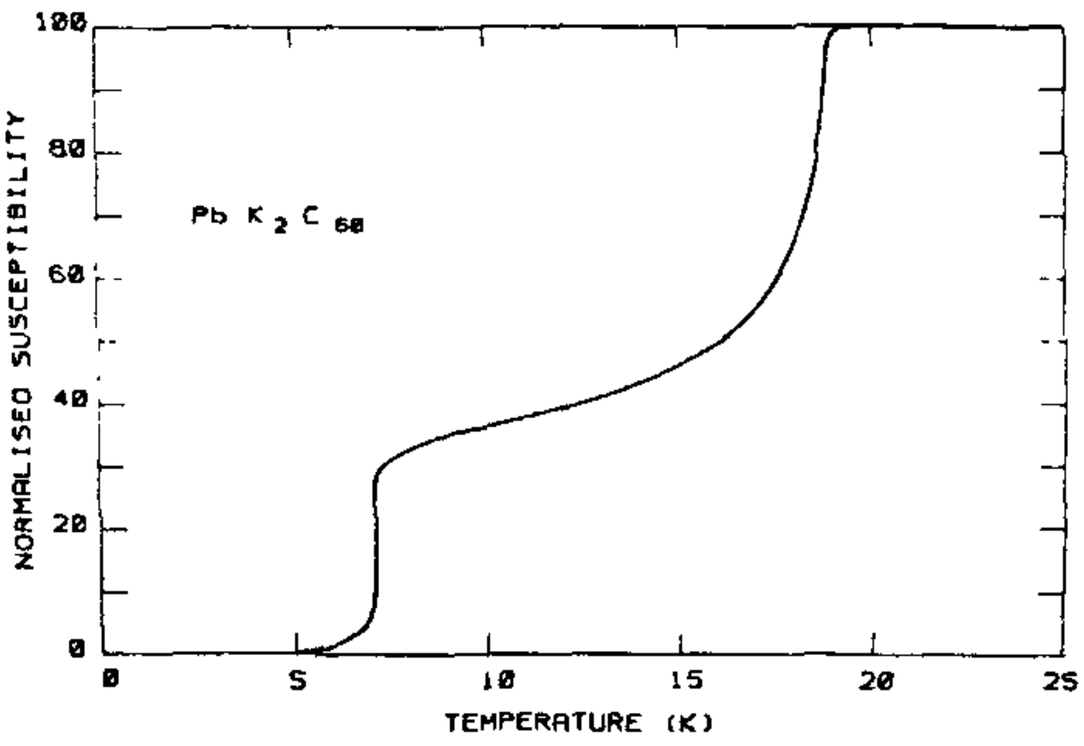

Figure 12. Normalized susceptibility versus temperature in PbK_2C_{60} showing superconducting transition at 18K. The transition in unreacted Pb is also seen.

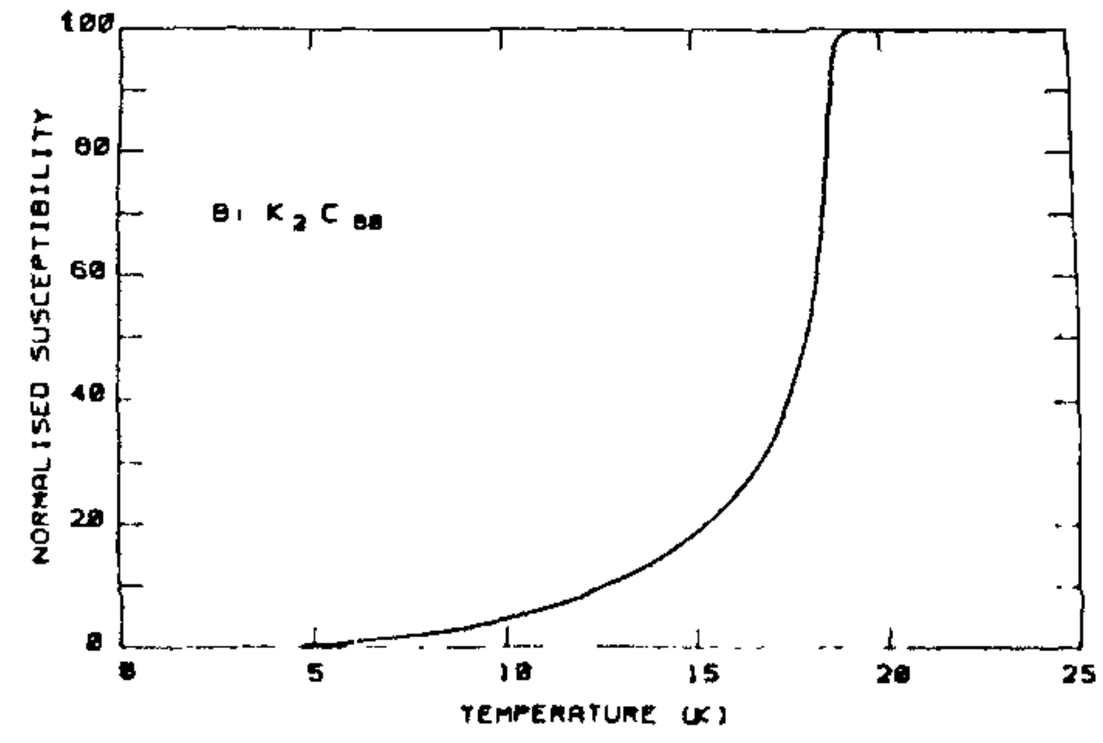

Figure 13. Normalized susceptibility versus temperature in BiK_2C_{60}.

expansion of the lattice. In the case of PbK_2C_{60}, the diffraction pattern can be indexed to an fcc structure with a few additional lines due to unreacted lead. The lattice constant of the fcc phase is estimated to be 14.18 Å. This is smaller than the lattice constant[11] of 14.25 Å corresponding to K_3C_{60}, even though the ionic radii of Pb (1.47 Å) is larger than K (1.39 Å). Comparing with the diffraction pattern of K_3C_{60}, shown in Figure 7, it is seen that the intensities of the (220) and (311) lines are inverted in the case of PbK_2C_{60}. This suggests partial substitution of Pb in place of K. In addition to X-ray diffraction, the samples have also been characterized by electron microprobe. These studies indicate that apart from localized pockets of unreacted Pb, Pb is uniformly distributed in the matrix. From a measurement of intensities of the K K_α to Pb M_α X-ray, the relative composition of Pb/K is estimated to be 1/10. Thus the composition of the Pb and K doped sample is estimated to be $K_{2.7}Pb_{0.3}C_{60}$.

In the case of Bi and K doped sample, the diffraction pattern can again be indexed to fcc with a lattice constant of 14.20 Å. From the additional lines due to Bi, it is estimated that about 5% of unreacted Bi is present. The relative intensities of the (220) and (311) lines (cf. Figure 7 for K_3C_{60}) also suggest the incorporation of Bi into the lattice.

Thus, from the experiments on co-doping Pb and Bi along with K, it is seen that while Pb and Bi are incorporated in the lattice as evinced from the diffraction results, there is no significant change in T_c compared to K_3C_{60}. Based on measured lattice parameters, and the established[35] correlation between T_c and lattice parameter, the T_c of the Pb/K and Bi/K doped samples would be expected at 17 K and 18 K respectively. Thus, lack of discernible change in T_c even in the Pb/K doped sample is intriguing. In order to understand these results, it will be important to obtain

definitive information on the lattice location of Pb and also to determine the charge state of the dopant by experimental techniques such as XPS. While the present results on lack of change in T_c with Pb and Bi doping may not be appealing, it may have significance in understanding the dramatic results[20] in Tl-doped C_{60}.

Studies on C_{70}

In contrast to the extensive studies on pristine and doped C_{60}, studies on C_{70} are almost non-existent. In view of this, we have undertaken detailed studies on the structural properties of C_{70}. A preliminary account of these results is presented in the following (see also ref. 40) and the details will be presented in subsequent publications.

Lattice statics calculations[41] indicate that the hcp structure is of lower energy compared to fcc and bcc for C_{70}. It may be noticed that C_{2v} is the largest crystallographic symmetry consistent with the D_{5h} symmetry of the C_{70} molecules. Therefore, the ground state of the C_{70} solid must be orthorhombic (or monoclinic/triclinic). Only at high temperatures, when the C_{70} molecules start rotating freely about their long axis does the symmetry get elevated to $D_{\infty h}$ and hcp become a possible structure. The experimental X-ray powder diffraction pattern of C_{70} is shown in figure 15. These have been indexed to orthorhombic structure with the lattice parameters, $a = 10.36$ Å, $b = 21.24$ Å, and $c = 30.10$ Å. From the measured density, it has been estimated that there are eight C_{70} molecules per unit cell. Detailed calculations of the structure factor and a comparison with the experimental diffraction pattern are in progress to identify the orientation of the C_{70} molecules within the unit cell[42].

Energy-dispersive X-ray diffraction measurements have been carried out in C_{70} as a function of truly hydrostatic pressure in the range of 0–20 GPa, using a diamond anvil cell. Dramatic changes in the diffraction pattern have been observed beyond 13 GPa and work is in progress to identify the high-pressure phase[42]. It may be remarked that in the case of C_{60}, having an fcc structure under ambient conditions, no structural transition has been observed under hydrostatic conditions up to 20 GPa, whereas only under nonhydrostatic conditions, a transition to crystallographic structure of lower symmetry is seen[32] at 16 GPa.

In the case of C_{60}, extensive studies on the development of orientational order at low temperature (249 K) and the concomitant change in structure from fcc to sc have been carried out using a variety of techniques such as X-ray diffraction[10], neutron diffraction[43], DSC[10,44] and NMR[45,31]. With a view to look for structural transition in C_{70} induced by temperature, X-ray diffraction experiments have been carried out as a function of temperature (under vacuum) up to 450°C. Apart from the shift of the peaks towards smaller angles due to thermal expansion, some of the diffraction peaks are seen to disappear. Work is in progress to identify the structural changes with temperature.

In addition to the studies on the structural properties of C_{70}, investigations on alkali metal doping of this system are also being carried out. Our studies[46] indicate that K and Rb-doped C_{70} are not superconducting. The implications of these results and further studies on doping of mixtures of C_{60} and C_{70} are underway.

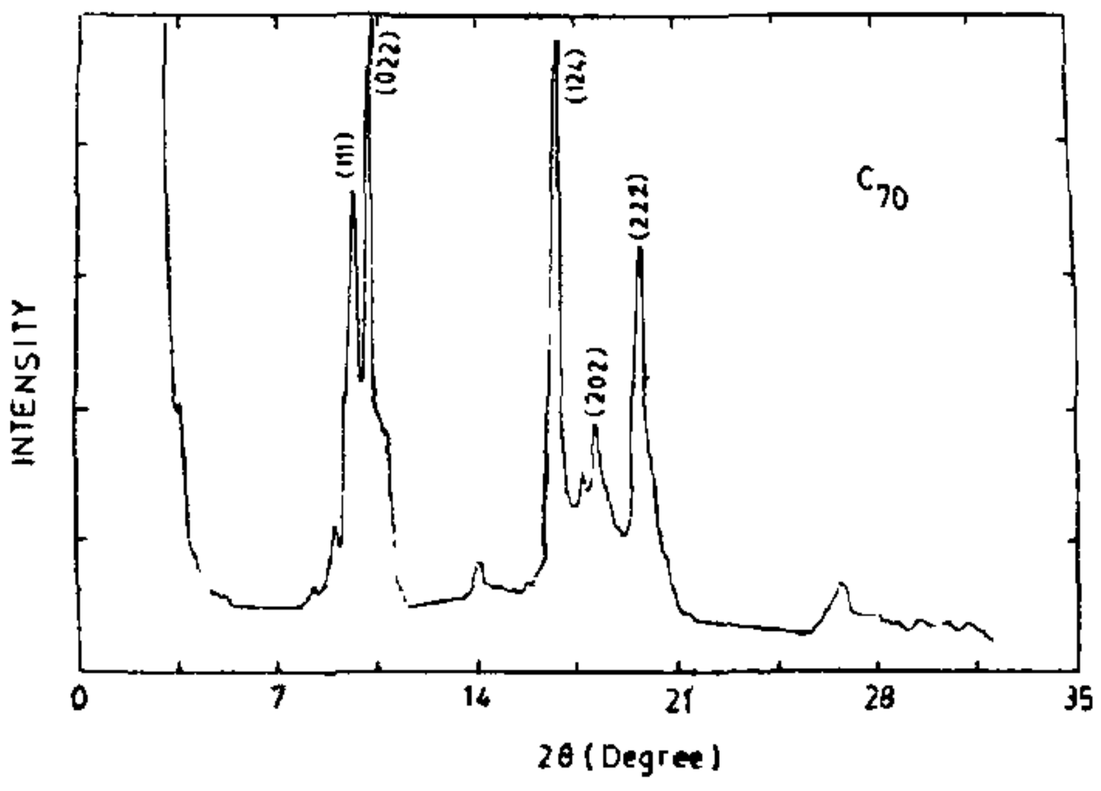

Figure 15. X-ray diffraction pattern of C_{70}. The lines have been indexed to orthorhombic structure.

Summary

The details of the arcing of graphite electrodes and chromatographic separation for the synthesis of pure C_{60} and C_{70} have been described. Doping of C_{60} with K and Rb results in superconducting samples with T_c of 18 K and 27 K respectively. Studies on Pb/K and Bi/K doped samples indicate that while Pb and Bi are incorporated into the lattice, there is no appreciable change in T_c as seen in the case of Tl doped sample. The preliminary results of on-going experiments on structural studies in C_{70} are also presented.

ACKNOWLEDGEMENTS. We thank Shri N. Chinnasamy for the skillful fabrication of the arcing apparatus and to Smt. M. Premila, Smt. Padma Gopalan and Kum. M. Shailaja for assistance in the chromatographic separation and UV-measurements. Thanks are also due to the members of the radiochemistry laboratory for discussions with regard to various aspects of chromatography. We are grateful to Shri K. Varatharajan and Dr A. K. Tyagi for lending their vacuum coating unit, which was modified into a fullerene generator during the first phase of experiments. The enthusiastic support and cooperation from various members of the Materials Science Division is gratefully acknowledged.

1. Kroto, H. W., Heath, L. R., O'Brien, S. C., Curl, R. F. and Smalley, R. E., *Nature*, 1985, **318**, 162.

2. Kratschmer, W., Lamb, L. D., Fostiropoulos, K. and Huffman, D. R., *Nature*, 1990, **347**, 354.
3. Haddon, R. C., *et al.*, *Nature*, 1991, **350**, 320.
4. Hebard, A. F., et al., Nature, 1991, **350**, 600.
5. Holczer, K. R., *et al.*, *Science*, 1991, **252**, 1154.
6. Rossiensky, M. J., *et al.*, *Phys. Rev. Lett.*, 1991, **66**, 2830.
7. Kelty, S. P., Chen, C. C. and Lieber, C. M., *Nature*, 1991, **352**, 223.
8. Chen, C. C., Kelty, S. P. and Lieber, C. M., Science, 1991, **253**, 886.
9. Tanigaki, K., *et al.*, *Nature*, 1991, **352**, 222.
10. Heiney, P. A., *et al.*, *Phys. Rev. Lett.*, 1991, **66**, 2911.
11. Stephens, P. W., *et al.*, *Nature*, 1991, **351**, 632.
12. Weaver, J. H., *et al.*, *Phys. Rev. Lett.*, 1991, **66**, 1741; Benning, P. J., Martins, J. L., Weaver, J. H., Chibante, L. P. F. and Smalley, R. E., *Science*, 1991, **252**, 1417.
13. Saito, S. and Oshiyama, A., *Phys. Rev. Lett.*, 1991, **66**, 2637.
14. Bethune, D. S., Meijer, G., Tang, W. C. and Rosen, H. J., *Chem. Phys. Lett.*, 1990, **174**, 219; Cappilletti, R. L., *et al.*, *Phys. Rev. Lett.*, 1991, **66**, 3261.
15. Prassides, K., *et al.*, *Nature*, 1991, **354**, 462; Duclos, S. J., Haddon, R. C., Glarum, S. H., Hebard, A. F. and Lyons, K. B., *Science*, 1991, **254**, 1625.
16. Holczer, K., *et al.*, *Phys. Rev. Lett.*, 1991, **67**, 271.
17. Uemera, Y. J., *et al.*, *Nature*, 1991, **352**, 605.
18. Zhang, Z., Chen, C. C., Kelty, S. P., Dai, H. and Lieber, C. H., *Nature*, 1991, **353**, 333; Zhang, Z., Chen, C. C. and Lieber, C. M., *Science*, 1991, **254**, 1619.
19. Rotter, L. D., *et al.*, *Nature*, 1992, **355**, 532.
20. Iqbal, Z., *et al.*, *Science*, 1991, **254**, 826.
21. Kortan, A. R., *et al.*, *Nature*, 1992, **355**, 529.
22. Parker, D. H., *et al.*, *J. Am. Chem. Soc.*, 1991, **113**, 7499.
23. Haufler, R. E., *et al.*, *J. Phys. Chem.*, 1990, **94**, 8634.
24. Pradeep, T. and Rao, C. N. R., *Mater. Res. Bull.*, 1991, **26**, 1101.
25. Howard, J. B., McKinnon, T., Makarovsky, Y., Lafleur, A. L. and Johnson, M. E., *Nature*, 1991, **352**, 139.
26. Arbogast, J. W., *et al.*, *J. Phys. Chem.*, 1991, **95**, 11.
27. Curl, R. F. and Smalley, R. E., *Sci. Am.*, 1991, (October), 54–63.
28. Mathews, C. K., *et al.*, *Curr. Sci.*, 1991, **61**, 834.
29. Ajie, H., *et al.*, *J. Phys. Chem.*, 1990, **84**, 8630.
30. Duclos, S. J., Haddon, R. C., Glarum, S. H., Hebard, A. F. and Lyons, K. B., *Solid State Commun.*, 1991, **80**, 481.
31. Tycko, R., *et al.*, *J. Phys. Chem.*, 1991, **95**, 518.
32. Duclos, S. J., Brister, K., Haddon, R. C., Kortan, A. R. and Thiel, F. A., *Nature*, 1991, **351**, 380.
33. Fleming, R. M., *et al.*, *Nature*, 1991, **352**, 701.
34. Zhou, O., *et al.*, *Nature*, 1991, **351**, 462.
35. Fleming, R. M., *et al.*, *Nature*, 1991, **352**, 787.
36. McCauley, Jr., J. P., et al., *J. Am. Chem. Soc.*, 1991, **113**, 8537.
37. Wang, H. H., *et al.*, *Inorg. Chem.*, 1991, **30**, 2838.
38. Benning, P. J., Martins, J. L., Weaver, J. H., Chibante, L. P. F. and Smalley, R. E., *Science*, 1991, **252**, 1417.
39. Tycko, R., *et al.*, *Science*, 1991, **253**, 884.
40. Sundar, C. S., *et al.*, *Indian J. Chem.*, 1992, (in print).
41. Guo, Y., Karasawa, N. and Goddard III, W. A., *Nature*, 1991, **351**, 464.
42. Yousuf, M., *et al.*, (under preparation).
43. Neumann, D. A., *et al.*, *Phys. Rev. Lett.*, 1991, **67**, 3808.
44. Samara, G. A., *et al.*, *Phys. Rev. Lett.*, 1991, **67**, 3136.
45. Yannoni, C. S., Johnson, R. D., Meijer, R. J., Bethune, D. S. and Salem, J. R., 1991, **95**, 9.
46. Hariharan, Y., *et al.*, Paper submitted to 'Superconductivity, Materials Physics and Applications', ICMAS-92, Houston, Texas, October 1992.

Climatology of long-period oscillations in the equatorial middle atmosphere over Thumba, India

S. C. Chakravarty, Jayati Datta and C. P. Revankar

Indian Space Research Organisation Headquarters, Bangalore 560 094, India

The reference middle atmospheric profiles of temperature, zonal/meridional winds have been derived for two successive periods of nine years each (1971–79, 1980–88) between 20 and 80 km from the regular meteorological rocket launches over Thumba (8°32'N, 76°52'E). The analysis of long-period oscillations from the 18-years data shows that there has not been any significant change in the pattern of these oscillations and temperature structure. There are considerable intercycle/interannual variations in the periods and amplitudes of quasibiennial oscillation (QBO) and interannual and intra-annual variations of semiannual oscillation (SAO). The yearly deviations of the peak SAO amplitudes from the climatological mean value and similar deviations of the area weighted annual rainfall amount over India are positively correlated with more than 95% confidence level. Higher values of SAO amplitudes are found to be associated with the westerly phase of QBO. Using the basic mechanism of equatorial wave-mean flow interactions, the characteristics of QBO and SAO have been explained. An attempt has been made to examine the results of the intercycle/interannual/intra-annual variations of the long-period oscillations based on these theoretical considerations.

UNDER Indo-USSR collaboration in space research, meteorological M-100 rockets are being launched once a week, on every Wednesday evening from Thumba